Molecular Cell, Vol. 5, 279–287, February, 2000, Copyright ©2000 by Cell Press

Capture and Visualization of a Catalytic RNA Enzyme-Product Complex Using Crystal Lattice Trapping and X-Ray Holographic Reconstruction

James B. Murray,* Hanna Szöke,† Abraham Szöke,† and William G. Scott*‡
*The Center for the Molecular Biology of RNA and
Department of Chemistry and Biochemistry
Sinsheimer Laboratories
University of California, Santa Cruz
Santa Cruz, California 95064
†Lawrence Livermore National Laboratories
L-30, 8000 East Avenue
Livermore, California 94551

Summary

We have determined the crystal structure of the enzyme-product complex of the hammerhead ribozyme by using a reinforced crystal lattice to trap the complex prior to dissociation and by employing X-ray holographic image reconstruction, a real-space electron density imaging and refinement procedure. Subsequent to catalysis, the cleavage site residue (C-17), together with its 2′,3′-cyclic phosphate, adopts a conformation close to and approximately perpendicular to the Watson-Crick base-pairing faces of two highly conserved purines in the ribozyme's catalytic pocket (G-5 and A-6). We observe several interactions with functional groups on these residues that have been identified as critical for ribozyme activity by biochemical analyses but whose role has defied explanation in terms of previous structural analyses. These interactions may therefore be relevant to the hammerhead ribozyme reaction mechanism.

Introduction

How does the three-dimensional structure of a ribozyme activate catalysis? To address this question, we and others (Pley et al., 1994; Scott et al., 1995) crystallized the hammerhead ribozyme and determined its initial state structure using X-ray crystallography. Although the self-cleavage reaction proceeds in crystals of the hammerhead ribozyme, allowing us to trap and observe two conformational intermediates that occur prior to catalysis (Scott et al., 1996; Murray et al., 1998a), the structure of the enzyme-product complex that forms subsequent to cleavage but prior to dissociation has never been observed. Upon cleavage, hammerhead ribozyme crystals become highly mosaic, making collection of useful diffraction data on the enzyme-product complex impossible (Scott et al., 1996). To solve this problem, we have now employed a reinforced version of the crystal lattice to trap the hammerhead enzyme-product complex and have determined its structure with the aid of a real-space electron density refinement procedure referred to as X-ray holographic reconstruction (Szöke, 1993).

‡To whom correspondence should be addressed (e-mail: wgscott@chemistry.ucsc.edu).

The hammerhead ribozyme (Prody et al., 1986; Uhlenbeck, 1987; Haseloff and Gerlach, 1988) is arguably the best-characterized ribozyme. Its small size, thoroughly investigated cleavage chemistry, known crystal structure, and its biological relevance make the hammerhead ribozyme particularly well suited for biophysical investigations. However, several other ribozyme and ribozyme fragment structures have now been elucidated. These include the structure of a folding domain of the group I intron (Cate et al., 1996) and the structure of a hepatitis delta virus self-cleaving RNA crystallized subsequent to cleavage and release of the 5′ region of the substrate (Ferre-D'Amare et al., 1998). In addition, a 5 Å resolution crystal structure of the group I intron catalytic core has emerged (Golden et al., 1998) that appears to agree in large part with previous careful molecular modeling studies (Michel and Westhof, 1990) and the structure of the previously determined folding domain. The structures of two domains of the hairpin ribozyme have been determined separately by NMR (Cai and Tinoco, 1996; Butcher et al., 1999). Finally, NMR (Hoogstraten et al., 1998) and crystal (Wedekind and McKay, 1998) structures of an in vitro selected ribozyme that cleaves in the presence of lead ion have been determined recently. Hence, our knowledge of catalytic RNA three-dimensional structures has been greatly improved in the last 5 years.

Our understanding of the relationship between the structure of catalytically active RNAs and their function (i.e., catalytic activity) remains more conjectural. The hammerhead ribozyme is still the only ribozyme whose catalytic activity has been characterized in terms of structural changes that take place in the crystal upon initiation of the self-cleavage reaction (Scott et al., 1996; Murray et al., 1998a), and it therefore offers the best hope of understanding how RNA structure activates catalysis. Despite the extensive structural and biochemical characterization of the hammerhead ribozyme (McKay, 1996; Wedekind and McKay, 1998), many important questions remain about how this RNA molecule's structure enables it to have catalytic activity.

The main features elucidated from the hammerhead ribozyme crystal structures are summarized in Figure 1. In particular, an absolutely conserved four-nucleotide loop, having the same sequence (CUGA) and structure (Pley et al., 1994) as the uridine turn found in $tRNA^{Phe}$, forms a catalytic pocket (Scott et al., 1995) into which the cleavage site base, C-17, is inserted. The exocyclic functional groups on A-6 and especially G-5 of the catalytic pocket are extremely sensitive to alteration (McKay, 1996). Removal of a G-5 exocyclic functional group can reduce the activity of the ribozyme 100- to 1000-fold. However, in the initial state (Pley et al., 1994; Scott et al., 1995) and conformational intermediate structures (Scott et al., 1996; Murray et al., 1998a), there are no direct contacts between these functional groups and the rest of the RNA. The remainder of the ribozyme, including the conserved residues that augment Stem II, apparently allows assembly of the ribozyme in such a way that serves to form the catalytic pocket and position

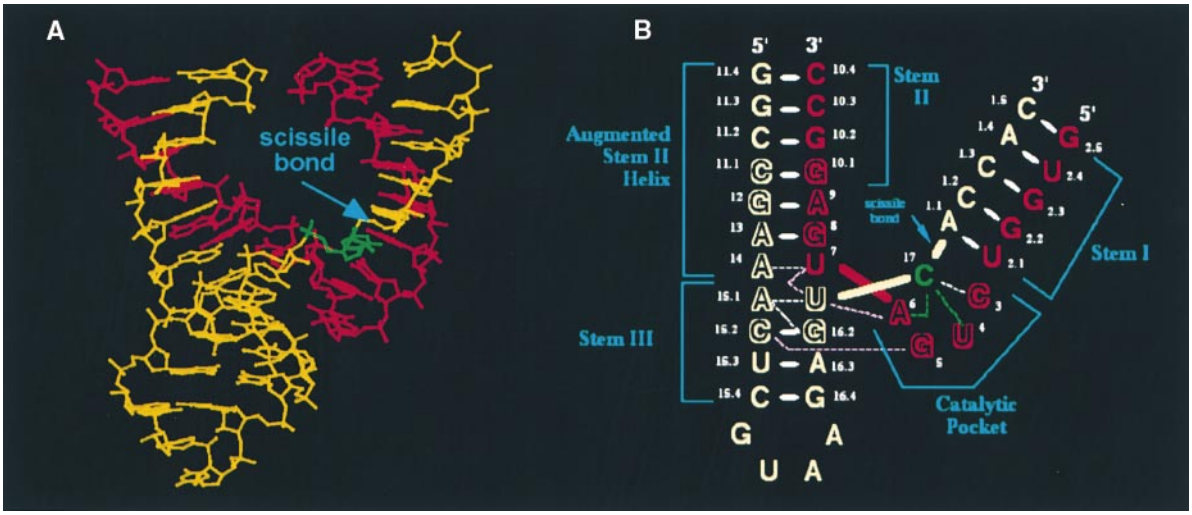

Figure 1. The Crystal Structure of the Hammerhead Ribozyme

(A) shows the three-dimensional crystal structure of the hammerhead ribozyme in its initial state conformation. (B) is a schematic diagram of this structure designed to complement (A). The enzyme strand is shown in red, the substrate strand in yellow, and the cleavage site base in green. Base pairing is indicated by white lines (with broken lines indicating noncanonical single H bond contacts), and pink lines indicate base–ribose interactions.

the cleavage site base in it. Some experiments appear to suggest that the conserved residues augmenting Stem II may also play a more direct role in the cleavage chemistry (Peracchi et al., 1997, 1998; Wang et al., 1999).

The initial state structures of the hammerhead ribozyme revealed that the scissile phosphate was in a conformation that was not compatible with the known $S_N2(P)$ or "in-line" attack mechanism of cleavage, in which the 2′-oxygen, the attacking nucleophile, is required to be in line with the phosphorus atom and the 5′-oxygen leaving group. In terms of a recently proposed fractional "in-line fitness" parameter (Soukup and Breaker, 1999), the initial state conformation of the scissile phosphate is quite incompatible ($F = 0.05/1.0$) with the $S_N2(P)$ mechanism. Hence, a conformational change that brings the scissile phosphate into a conformation more amenable to an in-line attack must take place for catalysis to occur.

Using a modified hammerhead RNA that cleaves slowly, we previously captured a conformational intermediate that is poised to form the in-line transition state (Murray et al., 1998a). This conformational change involved a 7 Å movement of the cleavage site base and ribose in such a way as to bring the 2′-oxygen attacking nucleophile into a geometry more compatible with future formation of an in-line transition state. The fractional in-line fitness parameter for the scissile phosphate in this conformation exceeds 1.0, indicating a potential contribution to catalysis exceeding the estimated 12-fold to 10^4-fold (Soukup and Breaker, 1999) rate enhancement predicted for a phosphate in the in-line conformation. Due to our modification of the leaving group, the actual transition state was essentially prevented from forming, but initiation of the cleavage reaction was unaltered. This allowed the conformational intermediate, stabilized by a relatively high pH of 8.5, to accumulate in the crystal under preequilibrium and pre-steady-state conditions and to be observed (Murray et al., 1998a). The conformational change that we observed permitted us to suggest that movement of the cleavage site base in such a way as to position the attacking nucleophile correctly for in-line attack formed the structural basis for hammerhead ribozyme catalysis (Murray et al., 1998a). However, this experiment could not reveal the force driving the conformational change, nor did it illuminate the roles of conserved bases in the catalytic pocket. Rather, it simply revealed how the ribozyme rearranged its conformation from that of the initial state structure to one allowing the required in-line attack to occur.

The principle of microscopic reversibility (Levine and Bernstein, 1987) states that the mechanisms for forward and back reactions in a simple reaction equilibrium must be identical. Therefore, the catalytic mechanism of the hammerhead ribozyme cleavage and ligation reactions must be the same, meaning that the sequence of events for the reverse reaction should be indistinguishable from those of the forward reaction when time is reversed. Because of this, the structure of the enzyme-product complex that forms just subsequent to cleavage of the ribozyme should be as relevant to the catalytic mechanism as is the structure of the conformational intermediate that forms just prior to cleavage. The Hammond postulate (Hammond, 1955; Le Noble et al., 1977; Miller, 1978) states that for endothermic reactions, such as the hammerhead cleavage reaction, the transition state structure will be more product-like than reactant-like. For these reasons, as well as for a complete structural characterization of the hammerhead ribozyme reaction pathway, the structure of the hammerhead ribozyme enzyme-product complex is of particular importance.

Results

Although the self-cleavage reaction proceeds in crystals of the hammerhead ribozyme, allowing conformational intermediates to be trapped and observed, the structure of the enzyme-product complex that forms subsequent

to cleavage but prior to dissociation has never been observed. Upon cleavage, crystals of the hammerhead ribozyme become disordered and the quality of X-ray diffraction deteriorates, thereby frustrating attempts to obtain the crystal structure of the enzyme-product complex (Scott et al., 1996). To circumvent the problem of crystalline disorder caused by RNA cleavage in the crystal, we have mixed a small percentage of modified (or inhibited) RNA substrate (Scott et al., 1995; Murray et al., 1998a) with unmodified RNA (Scott et al., 1996) during crystallization. This enables us to obtain crystals in which a known (and presumably randomly distributed) subset of the substrate molecules in the crystal are uncleavable or very slowly reactive. We find that this confers sufficient rigidity upon the crystal lattice to enable us to cleave the active RNA substrate in a standard single-turnover reaction under normal conditions without disrupting the diffraction properties of the crystal. In other words, we have strengthened the crystal lattice of the enzyme-product complex by randomly incorporating unreactive enzyme-substrate complex reinforcements and have thus used the crystal lattice itself to trap the enzyme-product complex before it becomes disordered.

A consequence of this "lattice trapping" experiment is that the electron density map we obtain will be a weighted average of the cleaved and uncleaved RNA structures. These must be deconvolved in a bias-free manner to enable us to observe the structure of the enzyme-product complex accurately. The conventional approach to doing so would be to employ residual omit-difference Fourier maps, using the uncleaved RNA as a model for generating crystallographic phases. However, this approach suffers from the fact that the phases are simply those of the nonomitted region of the structure. Consequently, the difference electron density that appears for the omitted region tends to be somewhat degraded in quality. Coupled with the partial occupancy of the cleaved structure, this has in practice made interpretation of standard omit-difference Fouriers rather difficult if comparatively large portions of the molecule change between the initial and final states of the reaction.

Because of the limitations of conventional residual difference Fouriers, we have turned to a previously developed technique that is based upon a formal analogy that can be made between the omit-map imaging procedure and holography (Szöke, 1993, 1998; Maalouf et al., 1993; Somoza et al., 1995, 1997; Szöke et al., 1997a, 1997b). Briefly, the part of the X-ray diffraction pattern generated by the known or nonomitted part of the structure is analogous to the "reference wave" in laser holography and that corresponding to the unknown or omitted part is analogous to the "object wave." By exploiting this analogy together with the constraint of maintaining the positivity of the electron density, highly reliable images of the entire molecule of the hammerhead ribozyme can be generated using less than one-fourth of the molecule to calculate the reference wave, as a test case. This result is consistent with several previous applications of the X-ray holographic methodology (Somoza et al., 1995, 1997; Szöke et al., 1997a, 1997b; Szöke, 1998). The phasing potential of the known part of the molecule is thus employed much more efficiently than can be done using the conventional residual difference Fourier procedure, making interpretation of omit maps for the purpose of identifying unknown structural elements or conformational changes much more reliable and straightforward.

Deterioration of the Hammerhead Ribozyme Crystals during Cleavage Can Be Prevented

By mixing unmodified, and therefore cleavable, hammerhead ribozyme substrate RNA with 25% to 50% RNA of the same sequence but possessing a cleavage site modification that inhibits cleavage (i.e., a 2′-F, 2′-OMe, or 5′-C-Me modification at the cleavage site), we have grown a series of crystals that remain intact under cleavage-active conditions but nevertheless have RNA that can be cleaved in proportion to the fraction of unmodified substrate RNA incorporated. Thus, the enzyme-inhibitor complex, presumably randomly incorporated throughout the crystal lattice with an occupancy approximately proportional to the fraction of inhibitor in solution, reinforces the crystal lattice, preventing disorder from occurring when the remainder of the RNA undergoes catalytic cleavage. The cleavage reactions were run under several sets of conditions, including those used previously for time-resolved crystallographic studies (Scott et al., 1996; Murray et al., 1998a) as well as a neutral pH condition using 25 mM $Cd(SO_4)$. Although the hammerhead ribozyme, when folded, does not require divalent cations for catalysis (Murray et al., 1998b), we have found that Cd^{2+} provides an unusually high (approximately 10-fold) enhancement of the rate of cleavage compared to all other conditions tested (J. B. M. and W. G. S., unpublished data).

We collected monochromatic X-ray cryocrystallographic data sets to 3 Å resolution on 12 hammerhead ribozyme crystals containing various quantities of substrate and inhibitor after the cleavage reactions were allowed to go to completion. The data were collected on a 2K CCD at Beamline X12C at Brookhaven National Laboratory National Synchrotron Light Source. Subsequently, these frozen crystals were transported back to the laboratory and assayed for extent of cleavage using HPLC as described previously (Murray et al., 1998a). The crystal having the greatest extent of cleavage that yielded processable X-ray diffraction data had undergone 60% cleavage (as assayed by HPLC UV absorbance integration, as shown in Figure 2) under conditions of 25 mM $Cd(SO_4)$, 1.8 M Li_2SO_4 in 50 mM HEPES (pH 7.0). A second crystal, in which 40% of the RNA was cleaved, produced X-ray data of good quality after having been subjected to the same cleavage conditions. The X-ray data for these crystals were refined against the previously determined initial state structure in this crystal form, and the resulting model was used to generate the initial phase set for electron density map calculation in XPLOR 3.8 and EDEN (see below and Table 1).

Hammerhead Ribozyme Electron Density Reconstruction Using the X-Ray Holographic Procedure

Because conventional residual difference Fourier techniques rely exclusively upon the phases of the known part of a structure, their utility for imaging structural

Table 1. Data Collection and Refinement Statistics

	40% Cleaved RNa	60% Cleaved RNA
Data collection[a]		
Cell (a, b, c in Å)	65.50 65.50 136.48	65.69 65.69 137.66
Resolution (Å)	24.618–3.105	19.782–3.125
Number of measurements	10825 (1455)	9814 (1395)
Number of unique reflections	6253 (834)	5371 (528)
Completeness	95.5% (91.3%)	85.8% (86.1%)
R_{scale}	10.4% (27.5%)	11.6% (38.0%)
<I>/Sigma I	7.4 (2.4)	5.4 (1.1)
Refinement		
R_{test} (90% of data)	25.8%	26.9%
R_{free} (10% of data)	32.1%	31.7%
rmsd bonds (Å)	0.011	0.012
rmsd angles (°)	1.972	1.732
rmsd torsion angles (°)	35.235	36.830
rmsd planar angles (°)	1.316	1.784

[a] Numbers in parentheses indicate values within the highest resolution bin.

changes, especially those that have only partial occupancy, is limited. Due to this limitation, more powerful techniques of image reconstruction would be particularly helpful in the task of producing interpretable electron density maps generated from partial structures. One such procedure, termed X-ray holography, uses the known part of the structure to calculate a "reference wave" and treats the remaining components of the observed X-ray structure factors as an "object wave," in analogy with laser holography.

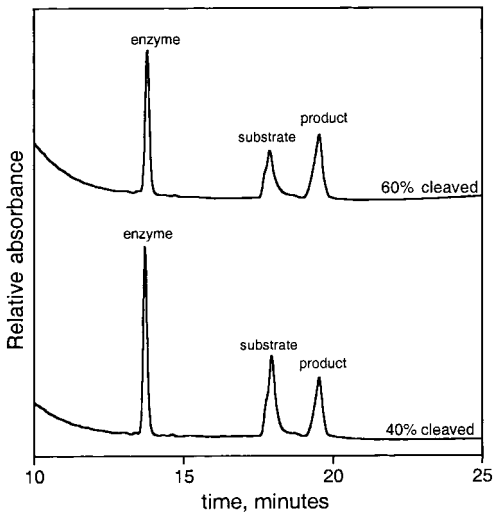

Figure 2. Hammerhead Ribozyme Cleavage in Crystals Having Mixtures of Cleavable and Uncleavable Substrates

The top HPLC chromatogram was obtained by dissolving the crystal used to obtain the structure in which 60% of the total substrate RNA had cleaved, and the bottom chromatogram was obtained from the crystal used to obtain the structure of the 40% cleaved RNA. As we observed in characterizing this assay previously (Murray et al., 1998a), the 25-mer RNA substrate elutes before the 20-mer RNA product, possibly due to the presence of the 2′,3′-cyclic phosphate terminus on the product strand. Standards containing either 100% cleaved substrate or 100% uncleaved substrate, as well as numerous time courses in which the substrate peak is observed to disappear as the product peak appears, verify the identity of these peaks.

Using the refined structure of the hammerhead ribozyme in its initial state (Scott et al., 1996) as a positive control, we tested the X-ray holographic procedure as implemented in the program EDEN (Somoza et al., 1995; Szöke et al., 1997a, 1997b) with the corresponding hammerhead ribozyme data set. By using less than one-fourth of the molecule to calculate the "reference" wave as a test case, we were able to recover interpretable electron density for the entire molecule, a result consistent with previous tests of the procedure (Somoza et al., 1995, 1997; Szöke et al., 1997a, 1997b; Szöke, 1998). The phasing potential of the known part of the molecule is thus employed much more efficiently than can be done using the standard residual difference Fourier procedure. We reasoned that if electron density maps generated in EDEN using less than one-fourth of this positive control structure revealed interpretable density for the entire molecule, then EDEN should be powerful enough to detect fairly large-scale changes that take place in crystals of the hammerhead ribozyme subsequent to partial cleavage, given coordinates for the uncleaved molecule and the unchanged parts of the cleaved molecule.

Crystal Structure of the Hammerhead Ribozyme-Product Complex

The X-ray holographic procedure has enabled us to detect and visualize a significant conformational rearrangement of the cleavage site base in the cleaved hammerhead RNA structure relative to the initial state structure, as is illustrated in Figures 3, 4, and 5. The same conformational change in the cleaved RNA was observed both in the crystal in which 60% of the RNA had cleaved and the crystal in which 40% of the RNA had cleaved. Instead of being positioned in the catalytic pocket as it is before cleavage, C-17 (the nucleotide 5′ to the scissile phosphate) moves dramatically in such a way as to be almost perpendicular to the Watson-Crick faces of G-5 and A-6 in the catalytic pocket. The three-dimensional arrangement of the cleaved RNA, with a 2′,3′-cyclic phosphate terminus generated by cleavage of the scissile phosphate, is shown in Figures 3

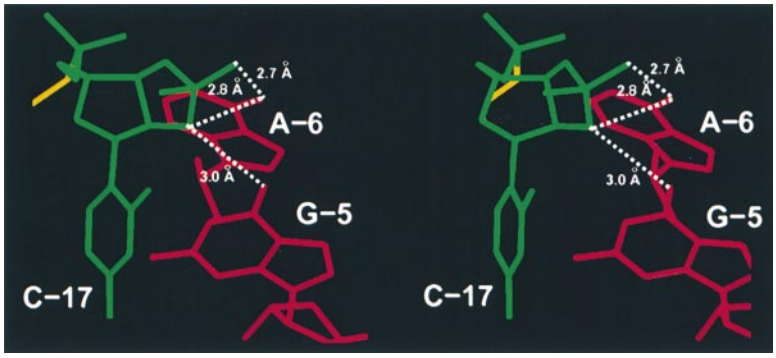

Figure 3. Stereo Image of the Cleavage Product

The 2′,3′-cyclic phosphate terminus of the ribozyme substrate complex is shown with various distances to the two closest residues of the enzyme strand, G-5 and A-6. Not all distances represent hydrogen bonds, as discussed in the text.

and 5, together with selected distances (not necessarily hydrogen bonds) between C-17, G-5, and A-6. It is apparent from the diagram (Figure 3) that several interactions between C-17 and these enzyme strand residues potentially exist. Most notable are the potential hydrogen bond that forms between the exocylic amine (N6) of A-6 and a cyclic phosphate nonbridging oxygen and the close approach of the keto oxygen (O6) of G-5 to the 2′-oxygen of C-17. These interactions are particularly interesting because they involve functional groups that reside on two residues (A-6 and G-5) that are quite critical for catalysis but whose importance cannot be explained by either the initial state or intermediate structures (McKay, 1996). Although the potential hydrogen bond forming between the cyclic phosphate of the product and the exocyclic amine of A-6 appears reasonable, neither the keto oxygen of guanine nor the 2′-oxygen of the cyclic phosphate are normally protonated; hence, there can be no hydrogen bond between them under ordinary circumstances. C-17 instead appears to form a perpendicular stabilizing aromatic interaction with G-5 that is reminiscent of what is often found in protein structures (Burley and Petsko, 1985). To form a hydrogen bond, either the 2′−oxygen would have to be protonated, or G-5 would need to exist as the enol tautomeric form. Both are unlikely for a stable enzyme-product complex under near-neutral pH conditions but may have some catalytic relevance as will be discussed below. The largest estimated rmsd coordinate errors for the atoms implicated in these interactions, based upon multiple independent simulated annealing refinements using different starting trajectories as well as a Luzzati analysis, are on the order of 0.25 Å, permitting a conservative estimation of the error associated with these measured distances of approximately ±0.5 Å.

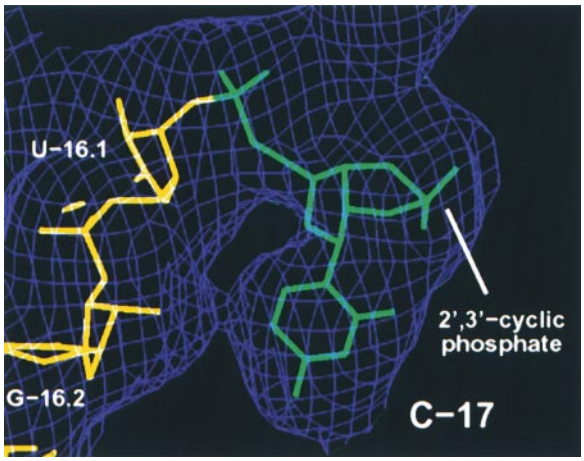

Figure 4. The EDEN Holographic Electron Density Map

The holographic reconstruction of the electron density of the hammerhead ribozyme cleavage product at 60% occupancy shows density that accommodates the 2′3′-cyclic phosphate terminus at C-17. The nucleotide and cyclic phosphate were omitted during map calculation. The additional density corresponds to the position of C-17 in the uncleaved substrate. (The holographic reconstruction procedure relies upon "apodization" or smearing of the data, which yields a map having more rounded features and thus gives the impression of being somewhat lower in resolution compared to the map below.)

Discussion

Implications for the Mechanism of Hammerhead Ribozyme Self-Cleavage

According to the Hammond postulate, transition state structures for endothermic reactions are more product-like, and those for exothermic reactions are more like reactants (Hammond, 1955). The hammerhead ribozyme cleavage reaction is somewhat endothermic but is spontaneous because of a large entropy gain realized upon cleavage (Hertel and Uhlenbeck, 1995). As a simple approximation, the enthalpic penalty paid in product formation is likely due to the formation of the cyclic phosphate, and the entropy gain that offsets this penalty arises primarily from relaxation of the enzyme-product complex subsequent to cleavage, and dissociation of the cleavage products from the enzyme strand of the ribozyme (as well as an R*ln*2 contribution from the production of two product strands from one substrate strand). This analysis permits us to suggest that some of the interactions observed in the enzyme-product complex may resemble those that occur in the transition state. Indeed, the most obvious manifestation of this effect is the resemblance of the 2′,3′-cyclic phosphate to a 2′,3′,5′-cyclic oxyphosphorane transition state.

At least two such potential transition state interactions should be considered, based upon the structure of the enzyme-product hammerhead ribozyme complex. First, the exocyclic amine of A-6 may hydrogen bond to one of the nonbridging oxygens of the pentacoordinated oxyphosphorane transition state, helping to dissipate

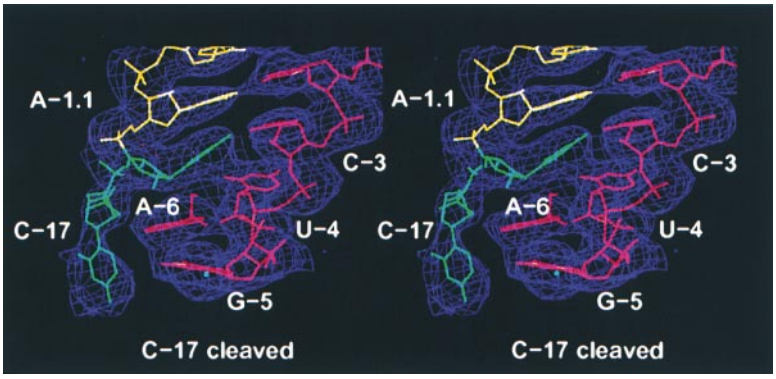

Figure 5. Stereo View of a Standard $2F_o - F_c$ Map

The map, calculated in XPLOR 3.8, shows reasonable density for the omitted, 40% occupied C-17 and its cyclic phosphate (shown in green). The density for the remainder of the catalytic pocket region is shown, including that for the uncleaved C−17 (also shown in green).

the accumulating negative charge. Evidence for a protonated, triester-like transition state structure has recently been presented (Zhou et al., 1998). Second, the potential interaction between G-5 and the 2′-oxygen of C-17 may also be of catalytic relevance if it persists in the transition state. The 2′-oxygen of C-17 in the substrate is initially protonated. If the 2′-H is transferred to O6 of G-5, the cleavage reaction might be initiated as G-5 transiently accepts a proton. Because the enol-like state of G-5 is unfavorable, this proton, or an N1 or N2 proton, would likely be surrendered to the solvent rather quickly, allowing restoration of the uncharged, keto state of G-5. The principle of microscopic reversibility can then be invoked to explain how the relatively rare back reaction is catalyzed. In addition to stabilization of the cyclic phosphate by the hydrogen bond to the exocyclic amine of A-6, the relatively rare keto-enol tautomerization of G-5 can potentially supply a proton to the 2′-oxygen in the (entropically unfavorable) event of nucleophilic attack by the 5′-terminal oxygen of residue 1.1 in the other product strand. Alternatively, the exocyclic amine may instead, or in addition, participate in transition state interactions that aid proton transfer in both the forward and back reactions in a form of anchimeric assistance. Although these mechanistic proposals have the merit of explaining the requirements for the G-5 and A-6 exocyclic functional groups, they do not address how the 5′-oxygen is stabilized during cleavage or how it becomes deprotonated when the ligation reaction is catalyzed. The crystal structure of a stable transition state analog that mimics the pentacoordinated oxyphosphorane will perhaps be best suited to answer these additional questions, as well as to test the mechanistic hypotheses we are presenting.

Terbium has been found to inhibit the hammerhead ribozyme cleavage reaction, and a combination of luminescence spectroscopy and X-ray crystallographic analysis has implicated a Tb^{3+} that binds to the Watson-Crick face of G-5 as being inhibitory (Feig et al., 1998). In this work, the authors proposed that Tb^{3+} may inhibit the cleavage reaction by preventing G-5 from making interactions required for catalysis. Our structure of the hammerhead ribozyme cleavage product, together with the Tb^{3+} experiments, permits us to suggest that Tb^{3+} inhibits cleavage by blocking C-17's interactions with G-5 and A-6 and thus provides some independent evidence that an interaction between C-17 and the exocyclic functional groups of these purines might be important for hammerhead ribozyme catalysis. The exocyclic amine of A-6 has also been found to be critical for catalysis by Ng et al. (1994), who found an approximate 100-fold cleavage rate reductions upon substitution with isoguanosine, 2-aminopurine or guanine. However, Fu and McLaughlin (1992) had previously found that substitution of A-6 with purine had only a minimal effect upon catalysis. The consensus on the importance of the exocyclic functional groups of G-5 is more uniform, with several groups (Fu and McLaughlin, 1992; Fu et al., 1993; Grabby et al., 1993; Tanaka et al., 1993; Tuschl et al., 1993; reviewed in McKay, 1996) agreeing that removal of either the exocyclic amine or oxygen decreases catalytic efficiency by at least 100-fold while increasing K_m on the order of 5-fold. It is therefore clear that the presence of the exocyclic functional groups on the purines of the

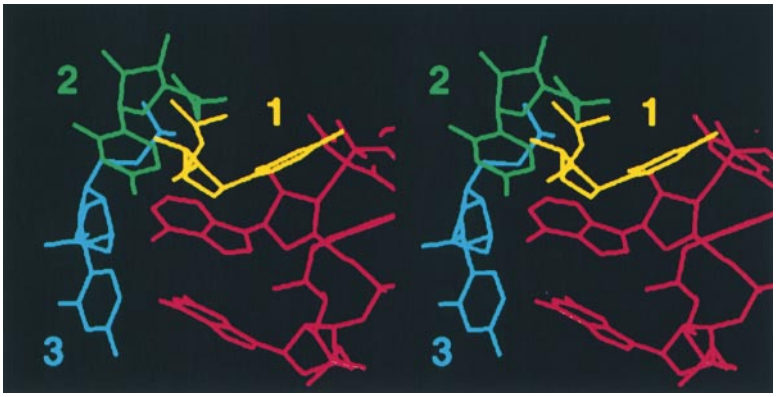

Figure 6. A Stereo Diagram that Depicts the Progress of the Cleavage Reaction

The enzyme strand is shown in red, and C-17 is shown in three different positions: the initial state structure in yellow, the later conformational intermediate structure in green, and the ribozyme-product complex structure in light blue. This gives an impression of the rather dramatic conformational dynamics that the ribozyme undergoes during catalysis.

catalytic pocket or domain I are associated with a two to four orders of magnitude rate enhancement of hammerhead catalysis, complementing the estimated one to four orders of magnitude rate enhancement provided by the in-line geometry of the scissile phosphate.

What is less clear is the role of the remaining conserved bases that augment Stem II (or the residues that compose domain II) in catalysis. It is clear that these residues are critical for forming the proper fold of the hammerhead ribozyme as has been discussed previously (Pley et al., 1994; Scott et al., 1995), but several modifications (reviewed in McKay, 1996) decrease the rate of catalysis by one or two orders of magnitude while having minimal effect upon the K_m. These results have been interpreted as implicating the remaining conserved bases more directly in catalysis. Although division between ground state and transition state effects of mutations can be problematic (Cannon et al., 1996), these results indicate either direct or at least indirect participation of the remaining conserved residues in formation of the transition state. Previously, we reported small conformational changes within the augmented Stem II helix in the transition from the initial state to the intermediate state structure (Murray et al., 1998a), including apparently tighter binding of a metal ion coordinated to the A-9-phosphate. We have also observed conformational heterogeneity in this region in two crystallographically independent molecules of the initial state structure in a different crystal form (Scott et al., 1995). However, in the current study, we have not attempted to deconvolve the initial state and cleaved state structures in this region, as this would involve refinement of a much larger set of parameters against the same number of measurements, making identification of small differences unreliable. Therefore, we are unable to provide any new insight into the catalytic role (if any) of the conserved nucleotides augmenting Stem II, as any such changes are small in magnitude compared to that observed for the cleavage site nucleotide (C-17).

In any case, we now have structures of the hammerhead ribozyme at several points on the self-cleavage reaction pathway. These include the initial state hammerhead structures, with both active and noncleaving or slowly cleaving substrates, all of which are essentially identical, as well as two freeze-trapped intermediate conformations that form prior to catalysis, and now the structure of the enzyme-product complex. Choosing the initial state structure, the later conformational intermediate structure, and the ribozyme-product complex structure, we can represent the rather dramatic reaction conformational dynamics with three superimposed structures as shown in Figure 6.

In summary, the structure of the hammerhead ribozyme enzyme-product complex, together with that of the conformational intermediate captured prior to cleavage (Murray et al., 1998a), enables us to propose that a conformational rearrangement of the cleavage site nucleotide during catalysis first involves positioning of the attacking nucleophile in-line with the 5′-oxygen leaving group of the RNA in a manner similar to that observed in the intermediate structure and, subsequently, may involve interactions between the scissile phosphate and ribose of C-17 and the exocyclic functional groups of G-5 and A-6. Our previous finding that the hammerhead ribozyme does not fundamentally require the presence of divalent metal ions in its cleavage chemistry (Murray et al., 1998b) entails that the RNA itself must possess the chemical properties that make catalytic self-cleavage possible. In this sense, a reaction mechanism requiring direct involvement of the critical functional groups contained in the catalytic pocket is particularly appealing. However, it must be pointed out that our proposal that the interactions that we observe in the enzyme-product complex are relevant to the transition state, even in the unlikely event of being correct in every detail, is still incomplete as it does not address the problem of how the 5′-oxygen leaving group is stabilized (or how a proton is abstracted to generate the 5′-oxygen attacking nucleophile in the reverse reaction). Nor does it explain the critical requirement for C-3 in catalysis. (It is however tempting to speculate, based on the proximity of C-3 to the 5′-terminal oxygen of the cleaved structure, that the two collaborate to provide additional catalytic power to the ribozyme.) Our crystallographic results also do not rule out a proposed mechanism in which the phosphate at A-9 and the scissile phosphate together coordinate a single metal ion (Peracchi et al., 1997, 1998; Wang et al., 1999), but based upon the constraints imposed by the crystal lattice and the lack of a strict requirement for a metal ion, the 20 Å rearrangement required by this metal-dependent mechanism is hard to reconcile with our current and previous results. This hypothesized conformational change can also be shown to contradict the results of several chemical crosslinking experiments (Murray and Scott, 2000).

Comparison of the solution NMR spectra of a cleaved and uncleaved form of the hammerhead ribozyme indicates that a significant structural change in the core region of the ribozyme takes place after cleavage (Simorre et al., 1997). The strongest evidence for this is the emergence of an NOE upon cleavage that indicates base pairing between U-4 of the catalytic pocket and U-7. These residues are about 10 Å apart in the initial state crystal structures; consequently, a significant conformational change must take place in solution subsequent to cleavage. Although we have not observed a direct interaction between U-4 and U-7, it must be remembered that in the case of the crystal structure of the hammerhead ribozyme-product complex, the crystal lattice has most likely trapped the cleaved RNA in a conformation that precedes formation of that observed in solution. Molecular dynamics calculations performed with the initial state crystal structure but augmented by the NMR data appear to indicate that G-5 is brought closer to the cleavage site nucleotide (Simorre et al., 1997). From the perspective of the crystal structure, the cleavage site nucleotide is brought closer to G-5, perhaps in a way that is consistent with these NMR-based predictions. In any case, the two sets of experiments are in agreement that a significant conformational change takes place upon cleavage, even if the results of these experiments do not agree in every detail.

Experimental Procedures

Crystallization of the Mixed RNA Crystals

Crystals containing various mixtures of unmodified (cleavable) and uncleavable hammerhead RNA molecules were grown using crystallization conditions previously reported (i.e., with 1 mM ribozyme in

50 mM NaOAc buffer [pH 5.0], 1.8 M Li_2SO_4 in the absence of Mg^{2+} and other divalent cations). The various strands of RNA were synthesized using oligoribonucleotide phosphoramidite chemistry, using deoxycytosine solid-phase supports. The RNA was purified successively by anion exchange HPLC and C-18 reverse-phase HPLC and subsequently desalted. We combined 4 μl of the RNA solution with 2 μl of reservoir solution (50 mM NaOAc [pH 5.0], 1.8 M Li_2SO_4, and 1.0 mM EDTA) and equilibrated as hanging or sitting drops against 0.75 ml of the reservoir solution sealed in a Linbro tissue culture plate at 16°C. The best crystals (0.2 × 0.2 × 0.3 mm) grew in these initially 6 μl drops rather than larger drops, formed within 2 to 3 days. The crystals were grown from mixtures containing unmodified hammerhead ribozyme substrate (Scott et al., 1996) or modified substrate (Scott et al., 1995; Murray et al., 1998a) at varying ratios (e.g., 1:3, 1:1, and 3:1 unmodified to modified substrate RNA). The actual extent of cleavage (and therefore likely the true ratio incorporated in the crystal) was subsequently assayed by HPLC (see below) as done previously (Murray et al., 1998a).

Collection of X-Ray Diffraction Data

Each crystal was soaked in a freezing solution consisting of 20% glycerol, 50 mM sodium cacodylate buffered at pH 6.5, 1.8 M Li_2SO_4, and 10 mM $CdSO_4$ for at least 200 min to ensure that cleavage to go to completion. In all cases, the soaking experiments were terminated by flash-freezing the crystals in liquid propane cooled in a bath of liquid nitrogen. Further details of data collection are described in Table 1.

Assay of the Extent of Cleavage

We assayed the cleavage in the crystal by HPLC as described previously (Murray et al., 1998a). Subsequent to data collection, crystals were thawed in a solution of 0.5 M EDTA and allowed to soak for 30 min before disrupting it and dissolving it in the EDTA solution. The sample was then analyzed at 50°C by ion exchange HPLC (Dionex DNA-PAC), using a gradient of 350 mM to 650 mM NH_4Cl in 30 min. Representative chromatograms are shown in Figure 2. Controls containing either 0% or 100% cleaved RNA were used to identify the locations of the substrate and product peaks.

Initial Refinement of the Data

Initial rigid-body refinement followed by conventional positional refinement (Powell minimization) in X-PLOR 3.8 (Brünger, 1993) was performed to refine a starting model for each RNA crystal structure. This starting model was then further refined using a standard simulated annealing slow-cooling molecular dynamics protocol followed by conventional positional and (highly) restrained temperature factor refinement in X-PLOR 3.8 using data from 8.0 Å to 3.0 Å resolution and a modified RNA geometry parameter library (Parkinson et al., 1996). This procedure lowered the R factor to about 27% in each case while maintaining very precise geometry. The cleavage site base (C-17), the scissile phosphate (of A-1.1) and residues 3–6 of the catalytic pocket were then omitted for a final round of simulated annealing refinement, and the coordinates of the remaining parts of the molecules were then used for constructing conventional ($2F_o - F_c$) and EDEN-based omit maps.

EDEN Holographic Reconstructions

Refined structures having the cleavage site base (C-17), the scissile phosphate (of A-1.1) and residues 3–6 of the catalytic pocket omitted from the last round of refinement were used as initial models for EDEN holographic construction in both correction mode and completion mode. A solvent target was prepared using the initial state ribozyme structure to construct a low-resolution solvent mask, and this was incorporated with a low (0.1) weighting in EDEN holographic electron density map reconstruction calculations. The maps were inspected at an rms cutoff of 0.4 to 0.6, as is typical for EDEN maps that are calculated on an absolute scale with positivity constraints on the electron density. Similar electron density features corresponding to the cleaved nucleotide (Figure 4) were observed in both the 40% cleaved RNA map and the 60% cleaved RNA map. A composite electron density map obtained from adding these two maps together and subtracting a third EDEN electron density map for the uncleaved structure (with the same nucleotides omitted) yielded what was essentially an averaged map of the cleaved structure at 100% occupancy (with the density for the uncleaved RNA subtracted out). Although this map was rather noisy, it clearly preserved the unique features assigned to the cleaved RNA. To further test the veracity of the EDEN electron density maps, conventional $2F_o - F_c$ maps for each crystal were constructed in XPLOR. Both maps are in agreement with the structure determined from the EDEN maps. The map corresponding to the 40% cleaved RNA (i.e., the weaker signal for the cleaved RNA) is shown in Figure 5. Hence, the structure for the cleaved crystal has been obtained in three ways using two independent X-ray crystal structures. These include the EDEN-generated electron density maps for each, the $\rho_{(100\%\ \text{cleaved})} = \rho_{(40\%\ \text{uncleaved})} + \rho_{(60\%\ \text{uncleaved})} - \rho_{(100\%\ \text{uncleaved})}$ electron density map, which is essentially an average of the two cleaved structures generated in EDEN, and two independent $2F_o - F_c$ maps calculated in XPLOR 3.8.

Final Refinement of the Structures

Following construction of a model for the cleaved RNA, the 40% cleaved and 60% cleaved RNA structures were refined using the standard protocol for treating multiple conformations in XPLOR 3.8. The occupancies of the cleaved and uncleaved substrate strands in the two crystals were set to those obtained from the HPLC assay, and a single enzyme strand having a 100% occupancy was employed in each case. To further minimize the number of independent variables to be refined, only nucleotides U-16.1, C-17, and A-1.1 were allowed to adopt two separate conformations. The 20-mer product strand was modeled with a 2′,3′-cyclic phosphate terminus having standard geometry, incorporated as a "patch residue" in XPLOR 3.8. Each structure was then refined to completion using the same protocol as outlined above. Finally, the low-resolution data were incorporated, and a solvent mask was determined and partial calculated structure factors were generated to model the bulk solvent contribution to the X-ray scattering amplitudes within X-PLOR 3.8. The structure was then further refined with all amplitudes from 43.0 Å to 3.1 Å resolution above 2σ, using the modeled bulk solvent.

Acknowledgments

We wish to thank F. Michel, H. F. Noller, and members of the Center for the Molecular Biology of RNA at the University of California, Santa Cruz, for inspiration, advice and criticisms, and the NIH for support (R01 AI43393–02). We thank L. Beigelman and Ribozyme Pharmaceuticals for synthesis of the 5′-C-methylated ribose substrate and Christine Dunham for assistance with data collection. Diffraction data for this study were collected at Brookhaven National Laboratory in the Biology Department single-crystal diffraction facility at beamline X12-C in the National Synchrotron Light Source with the helpful guidance of Robert Sweet and coworkers. This facility is supported by the United States Department of Energy Offices of Health and Environmental Research and of Basic Energy Sciences under prime contract DE-AC02–98CH10886, by the National Science Foundation, and by National Institutes of Health Grant 1P41 RR12408–01A1. We thank the W. R. Keck Foundation for support of RNA Center research at the University of California, Santa Cruz.

Received October 14, 1999; revised December 2, 1999.

References

Brünger, A.T. (1993). X-PLOR 3.1: A System for Crystallography and NMR (New Haven, CT: Yale University Press).

Burley, S.K., and Petsko, G.A. (1985). Aromatic–aromatic interaction: a mechanism of protein structure stabilization. Science *229*, 23–28.

Butcher, S.E., Allain, F.H., and Feigon, J. (1999). Solution structure of the loop B domain from the hairpin ribozyme. Nat. Struct. Biol. *6*, 212–216.

Cai, Z., and Tinoco, N. (1996). Solution structure of loop A from the hairpin ribozyme from tobacco ringspot virus satellite. Biochemistry *35*, 6026–6036.

Cannon, W.R., Singleton, S.F., and Benkovic, S.J. (1996). A perspective on biological catalysis. Nat. Struct. Biol. *3*, 821–833.

Cate, J.H., Gooding, A.R., Podell, E., Zhou, K., Golden, B.L., Kundrot,

C.E., Cech, T.R., and Doudna, J.A. (1996). Crystal structure of a group I ribozyme domain: principles of RNA packing. Science *273*, 1678–1685.

Feig, A.L., Scott, W.G., and Uhlenbeck, O.C. (1998). Inhibition of the hammerhead ribozyme cleavage reaction by site-specific binding of Tb(III). Science *279*, 81–84.

Ferre-D'Amare, A.R., Zhou, K., and Doudna, J.A. (1998). Crystal structure of a hepatitis delta virus ribozyme. Nature *395*, 567–574.

Fu, D.J., and McLaughlin, L.W. (1992). Importance of specific adenosine N7-nitrogens for efficient cleavage by a hammerhead ribozyme: a model for magnesium binding. Biochemistry *31*, 10941–10949.

Fu, D.J., Rajur, S.B., and McLaughlin, L.W. (1993). Importance of specific guanosine N7-nitrogens and purine amino groups for efficient cleavage by a hammerhead ribozyme. Biochemistry *32*, 10629–10637.

Golden, B.L., Gooding, A.R., Podell, E.R., and Cech, T.R. (1998). A preorganized active site in the crystal structure of the Tetrahymena ribozyme. Science *282*, 259–264.

Grabby, J.A., Jonathan, P., Butler, G., and Gait, M.J. (1993). The synthesis of oligoribonucleotides containing O6-methylguanosine: the role of conserved guanosine residues in hammerhead ribozyme cleavage. Nucleic Acids Res. *21*, 4444–4450.

Hammond, G.S. (1955). A correlation of reaction rates. J. Am. Chem. Soc. *77*, 334–338.

Haseloff, J., and Gerlach, W.L. (1988). Simple RNA enzymes with new and highly specific endoribonuclease activities. Nature *334*, 585–591.

Hertel, K.J., and Uhlenbeck, O.C. (1995). The internal equilibrium of the hammerhead ribozyme reaction. Biochemistry *34*, 1744–1749.

Hoogstraten, C.G., Legault, P., and Pardi, A. (1998). NMR solution structure of the lead-dependent ribozyme: evidence for dynamics in RNA catalysis. J. Mol. Biol. *284*, 337–350.

Le Noble, W.J., Miller, A.R., and Hamann, S.D. (1977). A simple, empirical function describing the reaction profile, and some applications. J. Org. Chem. *42*, 338–342.

Levine, R.D., and Bernstein, R.B. (1987). Molecular Reaction Dynamics and Chemical Reactivity (New York: Oxford University Press).

Maalouf, G.J., Hoch, J.C., Stern, A.S., Szöke, H., and Szöke, A. (1993). Holographic methods in X-ray crystallography. III. First numerical results. Acta Crystallog. A *49*, 866–871.

McKay, D.B. (1996). Structure and function of the hammerhead ribozyme: an unfinished story. RNA *2*, 395–403.

Michel, F., and Westhof, E. (1990). Modelling of the three-dimensional architecture of group I catalytic introns based on comparative sequence analysis. J. Mol. Biol. *216*, 585–610.

Miller, A.R. (1978). A theoretical relation for the position of the energy barrier between initial and final states of chemical reactions. J. Am. Chem. Soc. *100*, 1984–1992.

Murray, J.B., and Scott, W.G. (2000). Does a single metal ion bridge the A-9 and scissile phosphates in the catalytically active hammerhead ribozyme structure? J. Mol. Biol. *296*, 33–41.

Murray, J.B., Terwey, D.P., Maloney, L., Karpeisky, A., Usman, N., Beigelman, L., and Scott, W.G. (1998a). The structural basis of hammerhead ribozyme self-cleavage. Cell *92*, 665–673.

Murray, J.B., Seyhan, A.A., Walter, N.G., Burke, J.M., and Scott, W.G. (1998b). The hammerhead, hairpin and VS ribozymes are catalytically proficient in monovalent cations alone. Chem. Biol. *5*, 587–595.

Ng, M.M., Benseler, F., Tuschl, T., and Eckstein, F. (1994). Isoguanosine substitution of conserved adenosines in the hammerhead ribozyme. Biochemistry *33*, 12119–12126.

Parkinson, G., Vojtechovsky, J., Clowney, L., Brünger, A.T., and Berman, H.M. (1996). New parameters for the refinement of nucleic acid-containing structures. Acta Crystallog. *D52*, 57–69.

Peracchi, A., Beigelman, L., Scott, E.C., Uhlenbeck, O.C., and Herschlag, D. (1997). Involvement of a specific metal ion in the transition of the hammerhead ribozyme to its catalytic conformation. J. Biol. Chem. *272*, 26822–26826.

Peracchi, A., Karpeisky, A., Maloney, L., Beigelman, L., and Herschlag, D. (1998). A core folding model for catalysis by the hammerhead ribozyme accounts for its extraordinary sensitivity to abasic mutations. Biochemistry *37*, 14765–14775.

Pley, H.W., Flaherty, K.M., and McKay, D.B. (1994). Three-dimensional structure of a hammerhead ribozyme. Nature *372*, 68–74.

Prody, G.A., Bakos, J.T., Buzayan, J.M., Scheider, I.R., and Bruening, G. (1986). Autolytic processing of dimeric plant virus satellite RNA. Science *231*, 1577–1580.

Scott, W.G., Finch, J.T., and Klug, A. (1995). The crystal-structure of an all-RNA hammerhead ribozyme—a proposed mechanism for RNA catalytic cleavage. Cell *81*, 991–1002.

Scott, W.G., Murray, J.B., Arnold, J.R.P., Stoddard, B.L., and Klug, A. (1996). Capturing the structure of a catalytic RNA intermediate: the hammerhead ribozyme. Science *274*, 2065–2069.

Simorre, J.-P., Legault, P., Hangar, A.B., Michiels, P., and Pardi, A. (1997). A conformational change in the catalytic core of the hammerhead ribozyme upon cleavage of an RNA substrate. Biochemistry *36*, 518–525.

Somoza, J.R., Szöke, H., Goodman, D.M., Béran, P., Truckses, D., Kim, S.-H., and Szöke, A. (1995). Holographic methods in X-ray crystallography. IV. A fast algorithm and its application to macromolecular crystallography. Acta Crystallog. A *51*, 691–708.

Somoza, J.R., Szöke, H., and Szöke, A. (1997). Holographic methods in X-ray crystallography. NATO Advanced Study Institute on Direct Methods for Solving Macromolecular Structures (Erice, Italy).

Soukup, G.A., and Breaker, R.R. (1999). Relationship between internucleotide linkage geometry and the stability of RNA. RNA *5*, 1308–1325.

Szöke, A. (1993). Holographic methods in X-ray crystallography. II. Detailed theory and connection to other methods of crystallography. Acta Crystallog. A *49*, 853–866.

Szöke, A. (1998). Use of statistical information in X-ray crystallography with applications to the holographic method. Acta Crystallog. A *54*, 543–562.

Szöke, A., Szöke, H., and Somoza, J.R. (1997a). Holographic methods in X-ray crystallography. V. Molecular replacement, multiple isomorphous replacement, multiple anomalous dispersion and noncrystallographic symmetry. Acta Crystallog. A *53*, 291–303.

Szöke, A., Szöke, H., and Somoza, J.R. (1997b). Holographic methods in X-ray crystallography. CCP4 Daresbury Study Weekend Proceedings (http://www.dl.ac.uk/CCP/CCP4/proceedings/1997/a_szoke/main.html).

Tanaka, H., Hosaka, H., Takahashi, R., Imamura, Y., Takai, K., Yokoyama, S., and Takaku, H. (1993). Importance of specific purine-pyrimidine amino and hydroxyl groups for efficient cleavage by a hammerhead ribozyme. Nucleic Acids Symp. Ser. *1993*, 175–176.

Tuschl, T., Gohlke, C., Jovin, T.M., Westhof, E., and Eckstein, F. (1993). Importance of exocyclic base functional groups of central core guanosines for hammerhead ribozyme activity. Biochemistry *32*, 11658–11668.

Uhlenbeck, O.C. (1987). A small catalytic oligoribonucleotide. Nature *328*, 596–600.

Wang, S., Karbstein, K., Peracchi, A., Beigelman, L., and Herschlag, D. (1999). Identification of the hammerhead ribozyme metal ion binding site responsible for rescue of the deleterious effects of a cleavage site phosphorothioate. Biochemistry *38*, 14363–14378.

Wedekind, J.E., and McKay, D.B. (1998). Crystallographic structures of the hammerhead ribozyme: relationship to ribozyme folding and catalysis. Annu. Rev. Biophys. Biomol. Struct. *27*, 475–502.

Zhou, D.-M., He, Q.-C., Zhou, J.-M., and Taira, K. (1998). Explanatin by a putative triester-like mechanism for the thio effects and Mn^{2+} rescues in reactions catalytzed by a hammerhead ribozyme. FEBS Lett. *431*, 154–160.

Nucleic Acids Database ID Codes

Coordinates have been deposited with the Nucleic Acids Database, and ID codes will be available from the authors upon request.